Supplementary Information

On the Question of Steric Repulsion versus Noncovalent Attractive Interactions in

Chiral Phosphoric Acid Catalyzed Asymmetric Reactions

Soumi Tribedi,[a] Kazuo Kitaura,[b,c] Takahito Nakajima,[*,b] and Raghavan B. Sunoj[*,a]

[a]Department of Chemistry, Indian Institute of Technology Bombay, Powai, Mumbai 400076,

India

[b]RIKEN Center for Computational Science, 7-1-26 Minatojima-minami-machi, Chuo-ku,

Kobe, Hyogo 650-0047, Japan

[c]Fukui Institute for Fundamental Chemistry, Kyoto University, Takano-Nishihiraki-cho 34-4,

Sakyou-ku, Kyoto 606-8103, Japan

1. Theory: Pair Interaction Energy Decomposition Analysis (PIEDA)

The first step of the FMO method entails dividing the molecule into suitable fragments (total N). For fragments unconnected by covalent bonds, the segregation is simple, however, if otherwise, electrons are assigned to fragments such that the electrons paired in a bond are not separated (demonstration with both types of system are given in later sections). Thereby the FMO calculation begins with separate Hamiltonians for N number of closed shell fragments. The Hamiltonian for the Ith fragment is as follows:

$$H_I = \sum_i^{n_I} \left\{ -\frac{1}{2}\nabla_i^2 - \sum_s^{all\ atoms} \frac{Z_s}{|r_i - R_s|} + \sum_{J \neq I}^{N} \int dr' \frac{\rho_J(r')}{|r_i - r'|} \right\} + \sum_{i>j}^{n_I} \frac{1}{|r_i - r_j|} \dots (1)$$

where, n_I is the number of electrons in the fragment I, Z_s is the nuclear charge of atom s, $\rho_J(r)$ is the electron density distribution of fragment J. The first term in H_I is the kinetic energy of the electrons of Ith fragment, next is the attractive potential energy between electrons of Ith fragment and all the nuclei in the system, followed by the repulsive Coulomb potential between electrons of Ith fragment and that of the other fragments. The repulsive exchange energy is the last term, calculated over all electrons of the Ith fragment only. This fragment Hamiltonian differs from a Hartree Fock Hamiltonian by including the electrostatic potential from the electrons in the other fragments and the nuclear attractions from all the nuclei in the system.

Solution of the Schrödinger equation using this fragment Hamiltonian where the orbitals are localized within each fragment, affords the RHF energy of each fragment,

$$H_I \Psi_I = E'_I \Psi_I \dots (2)$$

Where, E'_I is the uncorrelated electronic energy of fragment I in the electrostatic field of the other fragments. For correlated methods, the density matrix of each fragment in the electrostatic field of other fragments, obtained from the FMO-RHF calculation, is used for

calculating the correlation energy for that particular fragment in any method of choice such as MP2, CC, DFT and so on. The total energy of the system, then, as calculated at the one-body FMO level (FMO1) is represented as a sum of the individual fragments. However, the FMO1 energy is not very accurate in recovering the total energy of the system. A two-body FMO calculation (FMO2) where energy and density of fragment pairs are also evaluated in the electrostatic field of the other fragments, is more accurate. Hence the fragment pair Hamiltonian is written as,

$$H_{IJ} = \sum_{i}^{n_I+n_J} \left\{ -\frac{1}{2}\nabla_i^2 - \sum_{s}^{all\ atoms} \frac{Z_s}{|r_i - r_s|} + \sum_{K \neq I,J}^{N} \int dr' \frac{\rho_K(r')}{|r_i - r'|} \right\} + \sum_{i>j}^{n_I+n_J} \frac{1}{|r_i - r_j|} \dots (3)$$

where, I and J are the two fragments. The corresponding Schrödinger equation which allows one to solve for energy of every fragment pair IJ is,

$$H_{IJ}\Psi_{IJ} = E'_{IJ}\Psi_{IJ} \dots (4)$$

and the FMO2 total energy of the system is given by,

$$E_{FMO2} = \sum_{I>J}^{N} E'_{IJ} - (N-2)\sum_{I}^{N} E'_I + \sum_{s>t}^{all\ atoms} \frac{Z_s Z_t}{|r_s - r_t|} \dots (5)$$

where, the last term is the nuclear repulsion energy between all the nuclei of the system. In our manuscript, we employ FMO2 energies everywhere.

The energy of any pair of fragments in the electrostatic field of all other fragments is obtained from the FMO calculation as shown in Eq. (4) along with the energy of each monomer fragment in the electrostatic field of other monomers as obtained from Eq. (2). Subtracting the constituent fragment energies from the energy of the fragment pair, leads to the pair interaction energy (PIE):

$$\Delta E_{IJ}^{int} = \left(E'_{IJ} - E'_I - E'_J \right) + Tr(\Delta \boldsymbol{D}^{IJ}\boldsymbol{V}^{IJ}) + \left(E_{IJ}^{corr} - E_I^{corr} - E_J^{corr} \right) \dots (6)$$

where E'_I and E_{IJ}' represent the monomer fragment and fragment pair RHF energies after subtracting the environment potentials V_I and V_{IJ}, respectively, i.e., $E_{IJ}' = E_{IJ} - \text{Tr}(\mathbf{D}^{IJ}\mathbf{V}^{IJ})$ where E_{IJ} is the total RHF energy of fragment pair *IJ*. D_I and D_{IJ} are the electron densities of monomer and dimer fragments respectively and E^I_{corr} and E^{IJ}_{corr} are the correlation energies of monomer and dimer fragments.

The interaction energy between each fragment pair is then divided into electrostatic (ΔE_{IJ}^{ES}), exchange-repulsion (ΔE_{IJ}^{ES}), charge transfer with higher order mixed terms ($\Delta Ect+mix$) and dispersion (ΔE_{IJ}^{DI}) components using EDA formalism:

$$\Delta E_{IJ}^{int} = \Delta E_{IJ}^{ES} + \Delta E_{IJ}^{EX} + \Delta E_{IJ}^{CT+mix} + \Delta E_{IJ}^{DI} \dots (7)$$

2. PIEDA Calculation: A Demonstration

The input for PIEDA calculation in GAMESS is prepared using a GUI fu-suite. We choose one small peptide FGG-114[1] as an example of an intramolecular system to demonstrate the step-by-step process.

a) The xyz format of the molecule is opened in fu program:
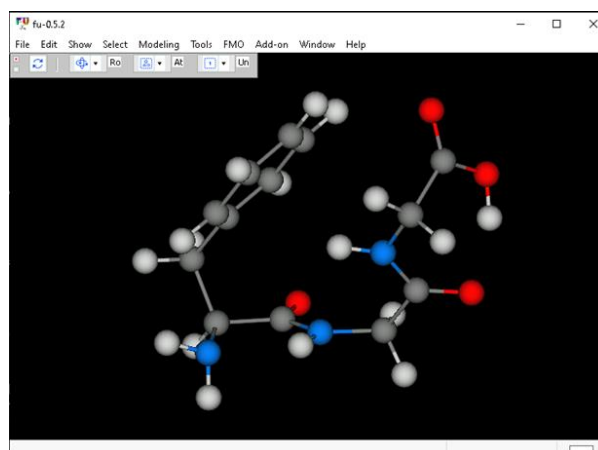
b) Click on 'FMO' tab, followed by 'Fragment tools' and then 'Manual BDA setting':

---

(1) Valdes, H.; Pluháčková, K.; Pitoňák, M.; Řezáč, J. and Hobza, P. *Phys. Chem. Chem. Phys.*, **2008**, *10*, 2747–2757.
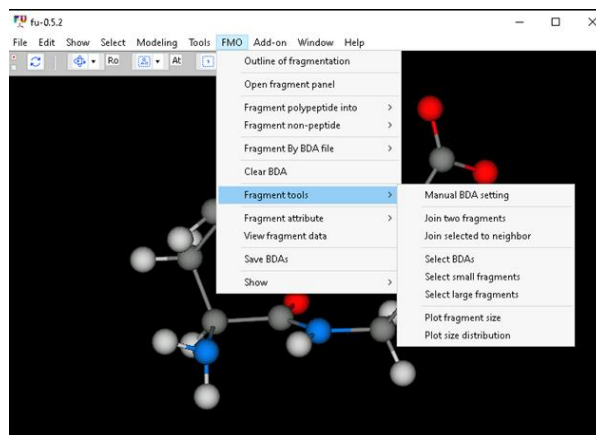
c)   Click on the atoms connecting the bond to be broken (highlighted in green in the figure below). The first atom to be selected becomes the bond dissociated atom (BDA):
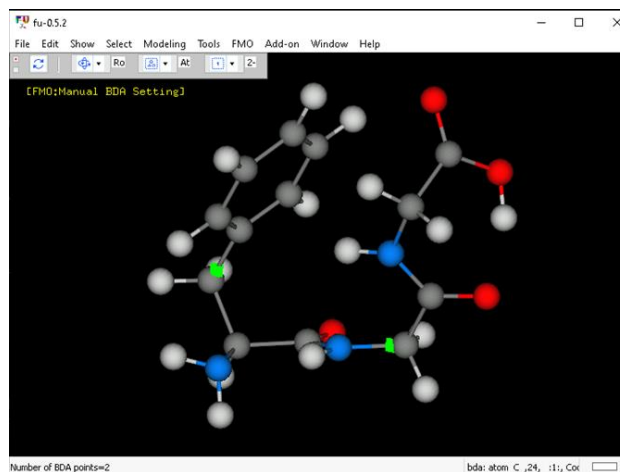
d) The fragments can be viewed by clicking the 'FMO' tab then selecting 'Show' followed by 'Paint Fragment'
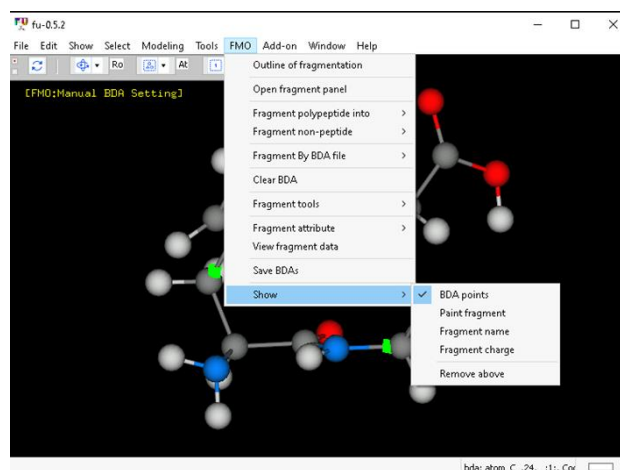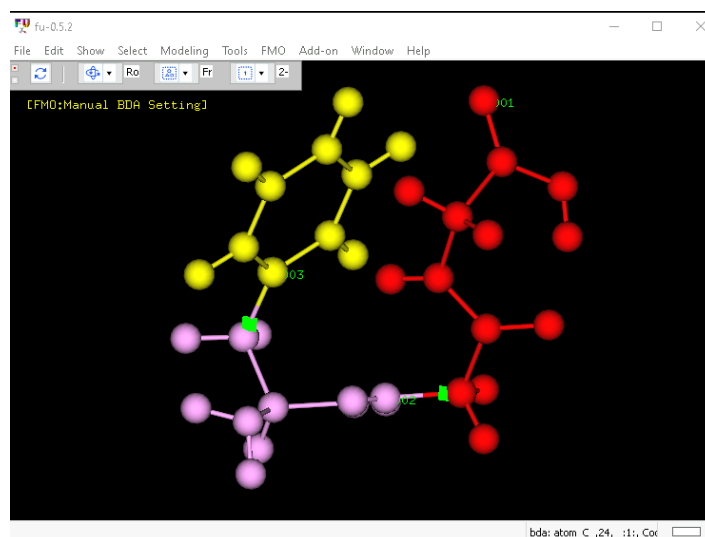
e) In order to prepare the input for gamess, click on 'Add-on' tab followed by 'gamess-user.py' from the menu. This will open up a dialogue box as shown below

f) Select 'FMO' from the dropdown menu of Method, change charge or multiplicity as required, click on FU tab to get the coordinates from the molecule in the viewing window. Next, the wavefunction type can be selected followed by the basis set (in this case M06-2X and 6-31G** respectively). Then click on the 'Save' tab to save the .inp file

S7
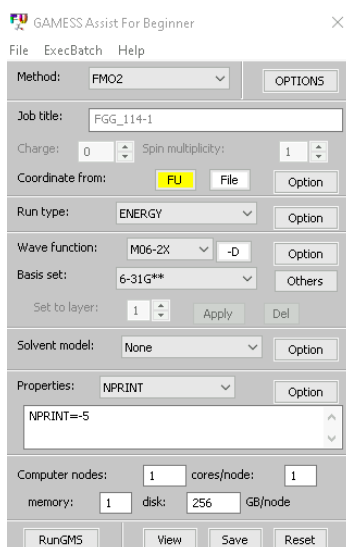
3. Interaction Energies Calculated Using Espinosa's Formalism and F-sSAPT

The interaction energies between the substrate and 3,3'-fragments in our study were also evaluated using Espinosa formalism which uses the topological quantities derived from Atoms-in-Molecules analysis to evaluate the energies associated with each contact identified by AIM. Energies for various types of contact between two particular fragments were summed together (Table S1) and plotted against the PIEDA interaction energies for the same fragment pairs (Figure S1). In addition, Sherrill's exchange-scaled functional group symmetry adapted perturbation theory (F-sSAPT) has been employed as well for comparison.

Table S1. Estimated Strength of NCIs Between Fragment Pairs Calculated using PIEDA, Espinosa and F-sSAPT in kcal/mol.

Fragment Pairs	PIEDA	Espinosa	F-sSAPT
TS-I-S-A	-7.7	-8.3	-3.8
TS-I-S-B	-8.1	-7.6	-5.6
TS-I-R-A	-4.3	-1.4	-2.3
TS-I-R-B	-9.8	-6.9	-6.6
TS-IIa-R-A	-16.3	-37.2	1.0
TS-IIa-R-B	-16.3	-33.6	-0.8
TS-IIa-S-A	-16.3	-29.1	-1.2
TS-IIa-S-B	-18.8	-28.1	-0.7
TS-IIb-R-A	-19.3	-8.9	-6.8
TS-IIb-R-B	-22.3	-18.4	-8.6
TS-IIb-S-A	-13.8	-5.6	-6.9
TS-IIb-S-B	-30.8	-20.6	-9.1

TS-IIIa-S-A	-20.6	-15.5	-17.7
TS-IIIa-S-B	-4.5	-2.2	-4.6
TS-IIIb-R-A	-3.9	-0.4	-4.8
TS-IIIb-R-B	-23.6	-12.5	-20.8

The largest differences in the interaction energies between the three quantification methods used here are found in the case of reactions **IIa** and **IIb**. The Pearson's correlation coefficient (R) is listed in Table S2 for all the reactions as well as after excluding reactions **IIa** and **IIb**. Notable improvement is evident in the R-values after the exclusion of said reactions, the best being $R_{PIEDA-Espinosa}$ = 0.93. However, F-sSAPT displays poor correlation with both PIEDA and Espinosa's methods. This might be attributed to the fact that the exchange-scaling factor in F-sSAPT has been optimized to reproduce total interaction energies, which is proposed to have accuracy issues with the fragment-fragment interaction energies.[2] Reactions **IIa** and **IIb** involve highly conjugated aromatic fragments as compared to the other reactions. The number of bonds involved in the coupled reaction coordinate is 5 in reaction **I**, 4 in reactions **IIIa** and **IIIb**, whereas it is 7 in reactions **IIa** and **IIb** (excluding the O–P–O part of phosphate which is also involved in RC but common in all the TSs as shown in Scheme 1). It might lead to higher contribution of the exchange term than currently accounted for in both PIEDA and F-sSAPT methods, thus leading to a larger difference in the computed values.

Table S2. Pearson's Correlation Coefficient Between PIEDA Interaction Energies and Those Obtained from Additive Espinosa's Formalism and F-sSAPT

Correlation coefficient	**All reactions**	**Excluding IIa and IIb**
$R_{PIEDA-Espinosa}$	0.56	0.93
$R_{PIEDA-F-sSAPT}$	0.44	0.70
$R_{Espinosa-F-sSAPT}$	-0.29	0.58

---

(2) http://forum.psicode.org/t/ssapt-scaling-term-and-f-sapt/1321/3, accessed on 04/05/2021.

The inconsistency of F-sSAPT results for reaction **IIa** might also be due to the general issues with the basis set of fluorine atom.[3] Since SAPT0 has been reported to work best with jun-cc-pVDZ basis set,[4] we also reevaluated the F-sSAPT results using the calendar basis set for all atoms in the case of reaction **IIa**. However, the interaction energies in **TS-IIa-R-A**, **TS-IIa-R-B**, **TS-IIa-S-A**, **TS-IIa-S-B** amount to 0.5, -0.9, -1.2, -1.4 kcal/mol respectively, which are at variance with the other methods.

The interaction energies for each contact type (i.e. C–H⋯O, C–H⋯π etc.) as obtained using the Espinosa formalism are summed together and compared in Figure S1. This allows us to evaluate the relative contribution of each type of interaction to the total. The C–H⋯O contacts offer significant percentage of the stabilization in **TS-I-S** whereas it is predominantly C–H⋯π in **TS-I-R**. It is interesting to note that in reaction **IIa**, the predominant stabilizing interactions are C–F⋯O and C–H⋯F (Figure S2(b) for Espinosa quantification), where the substituent is -$(CF_3)_2C_6H_4$ and C–H⋯π and lp(O)⋯π with the anthryl substituent in reaction **IIb**. Further, for the methyl oxetane system, C–H⋯π appears to be significant and the strength decreases when the substrate is hydroxy oxetane.

(3) (a) Hickey, A. L.; Rowley, C. N. *J. Phys. Chem. A* **2014**, *118*, 3678. (b) Jaszuński, M.; Świder, P.; Sauer, S. P. A. *Mol. Phys.* **2019**, *117*, 1469. (c) Siiskonen, A.; Priimagi, A. *J. Mol. Model* **2017**, 23:50.

(4) (a) Bakr, B. W.; Sherrill, C. D. *Phys. Chem. Chem. Phys.* **2016**, *18*, 10297. (b) Bakr, B. W.; Sherrill, C. D. *Phys. Chem. Chem. Phys.* **2018**, *20*, 18241.

a)
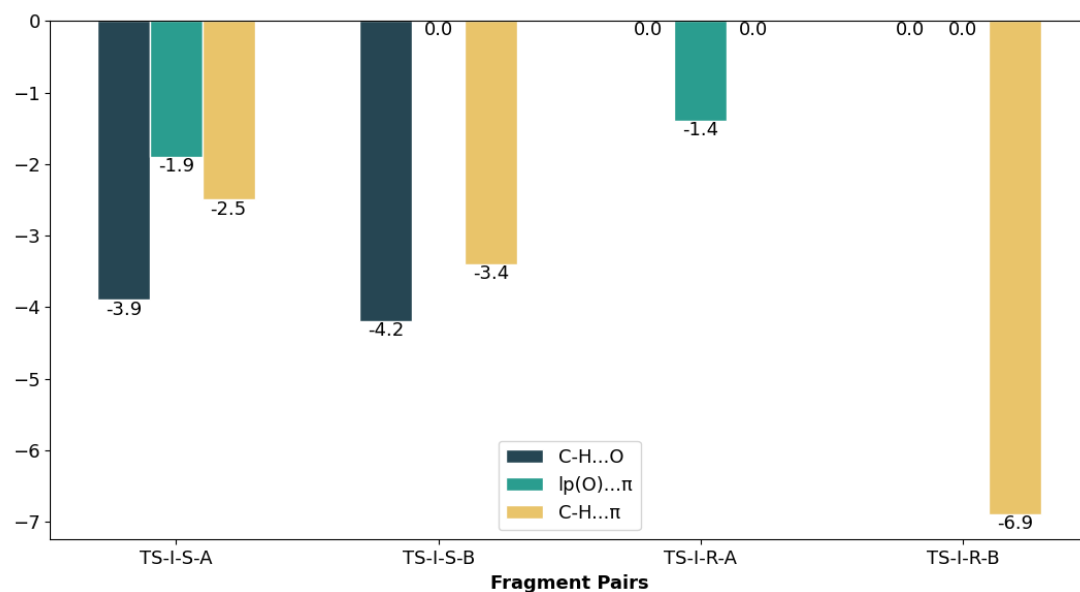
b)
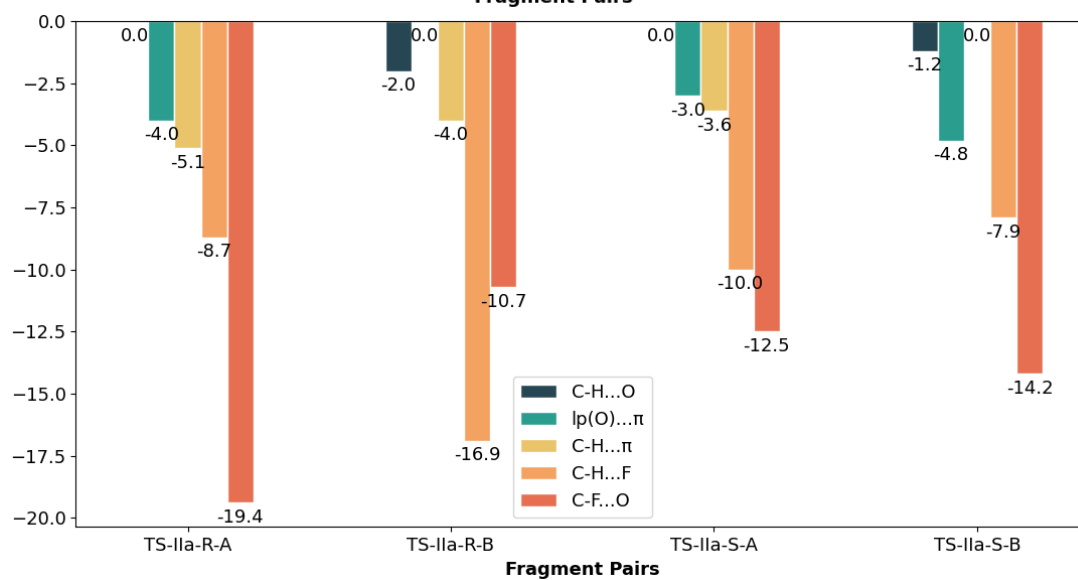
Figure S1 continued…

c)

d)
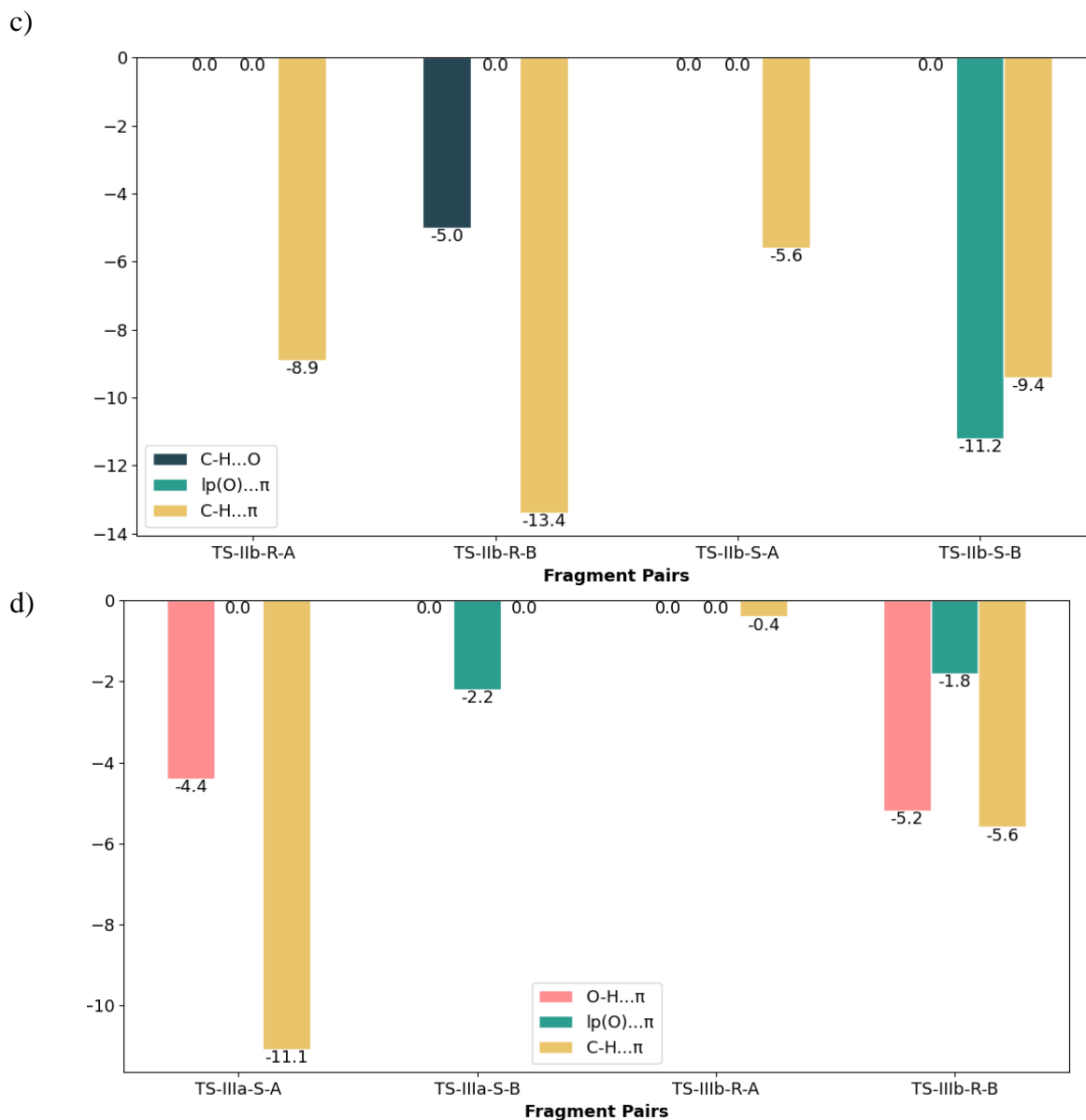
Figure S1. The interaction energies between fragments of the stereocontrolling TSs of a) reaction **I**, b) reaction **IIa** c) reaction **IIb**, and, d) reaction **IIIa** and **IIIb** calculated using the Espinosa formalism segregated into types of interactions.

4. Interaction Energies and Its Components Between Substrates and Catalyst Fragments as Calculated by F-sSAPT

As a contemporary method which have been employed for evaluating intramolecular interactions in TSs, we have compiled the F-sSAPT data at the 6-31G** basis set for the

same systems. Although the quantities of interactions do not exactly match with PIEDA, the trend and relative contribution of energies remain similar in both methods.

a)

b)
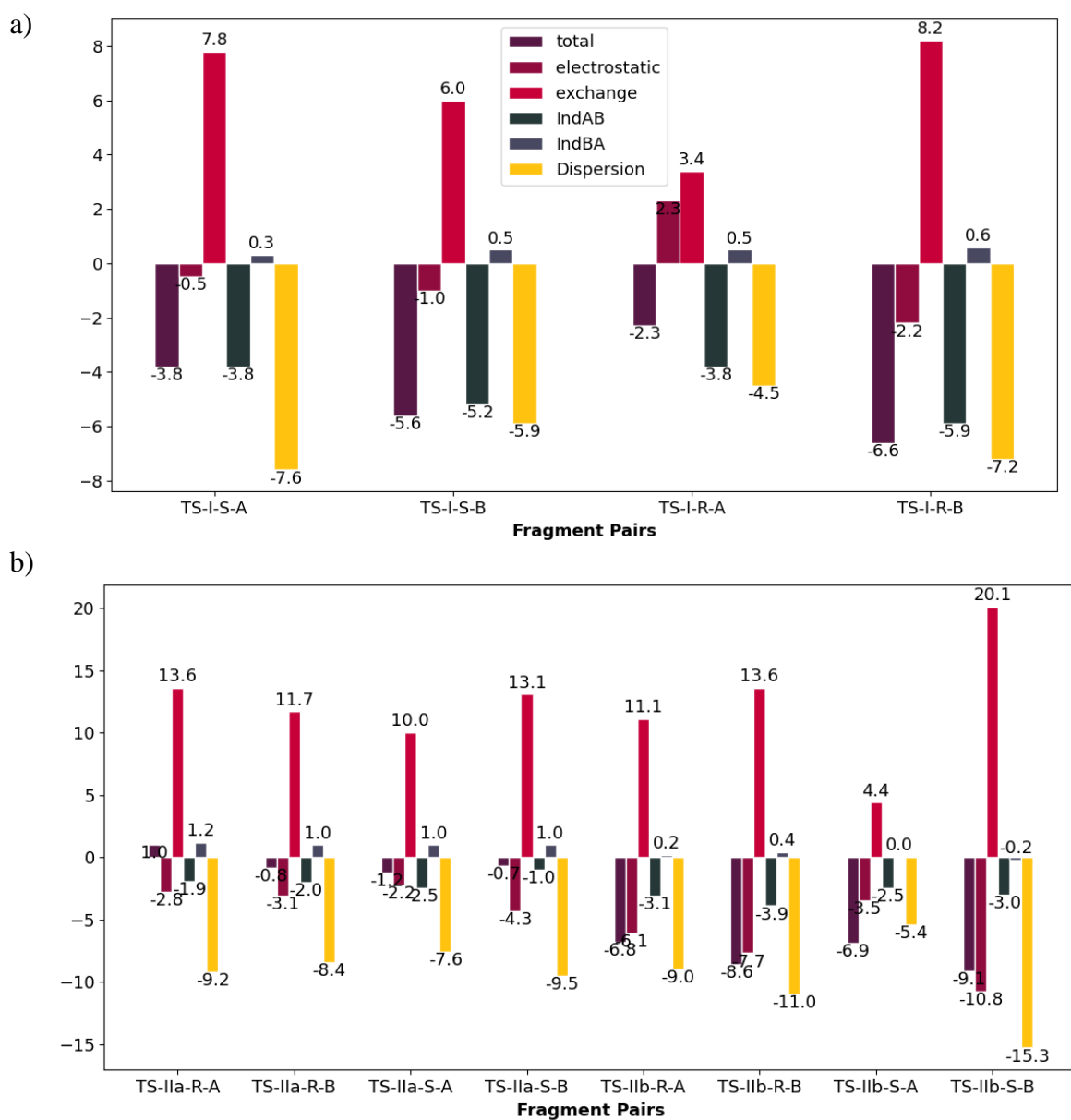
Figure S2 continued…

c)
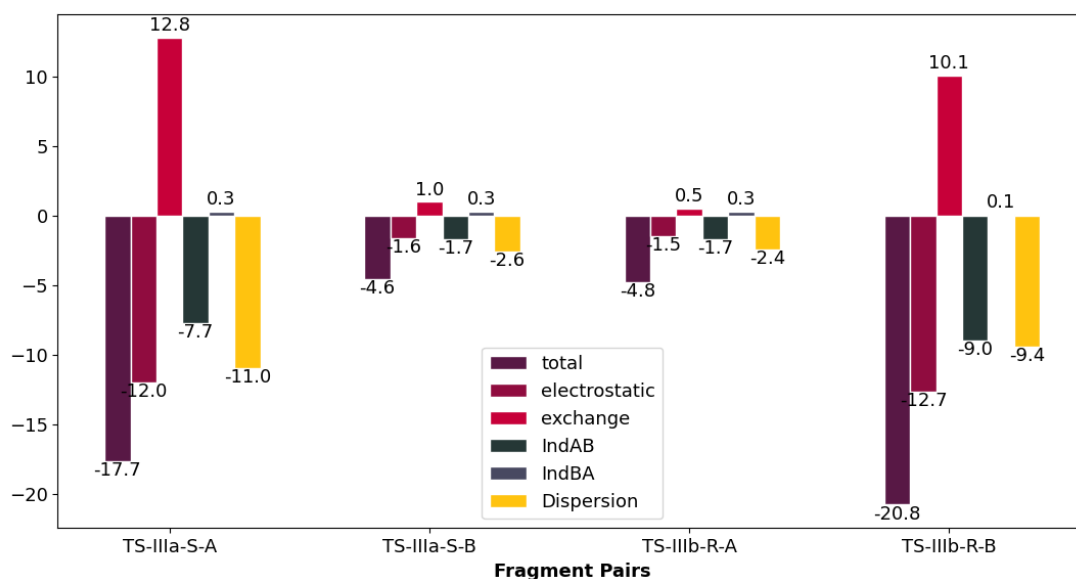
Figure S2. The interaction energy and its components between fragments of the stereocontrolling TSs of a) reaction **I**, b) reaction **IIa** and **IIb**, and, c) reaction **IIIa** and **IIIb** calculated using F-sSAPT/6-31G**.

5. Intermolecular Interaction Energies in Model Systems

a)   C–H···O

-1.3 (-0.7)
-1.3 (-0.7)

b)   C–H···π

-1.6 (-1.1)
-1.9 (-1.3)

c)   O–H···π

-4.2 (-3.3)
-4.3 (-3.4)

d)   lp(O)···π

-4.7 (-2.9)
-4.9 (-3.0)

e)   C–F···O

-3.1 (-0.4)
-3.4 (-0.7)

f)   C–H···F

-2.3 (-0.6)
-2.3 (-0.7)
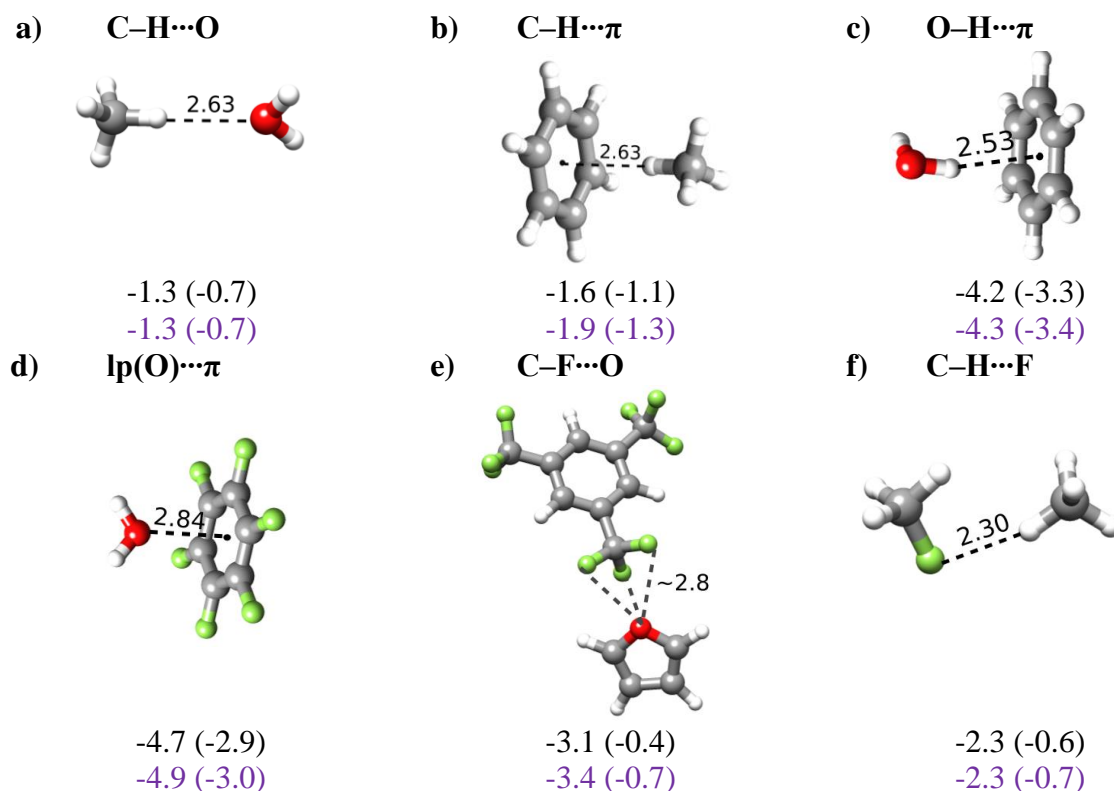
Figure S3. Model binary systems bound primarily through a) C–H···O, b) C–H···π, c) O–

H···π, d) lp(O)···π, e) C–F···O, and f) C–H···F interactions, which are shown using dotted lines. The distances are in Å and the interaction energies are in kcal/mol, calculated at the M06-2X/6-31G** level of theory (in black) and M06-2X-D3/6-31G** (in purple). The counterpoise corrected values are provided in parenthesis.

Table S3. The Interaction Energies and Its Components Calculated using FMO2-PIEDA for Model Systems

Interaction Type		Level of theory	Total	Elst.	Exch.	Ect+mix	Disp.
a)	**C–H···O**	M06-2X/6-31G**	-1.4	-0.9	1.0	-0.8	-0.7
		M06-2X-D3/6-31G**	-2.0	-0.9	1.0	-0.8	-1.3
b)	**C–H···π**	M06-2X/6-31G**	-1.7	-0.7	3.1	-0.6	-3.5
		M06-2X-D3/6-31G**	-4.3	-0.7	3.1	-0.6	-6.1
c)	**O–H···π**	M06-2X/6-31G**	-4.5	-3.3	3.5	-1.3	-3.3
		M06-2X-D3/6-31G**	-7.1	-3.3	3.5	-1.3	-6.0
d)	**lp(O)···π**	M06-2X/6-31G**	-5.1	-3.8	5.7	-1.4	-5.6
		M06-2X-D3/6-31G**	-7.9	-3.8	5.7	-1.4	-8.4
e)	**C–F···O**	M06-2X/6-31G**	-3.1	-1.0	5.8	-2.2	-5.7
		M06-2X-D3/6-31G**	-6.4	-1.0	5.8	-2.2	-9.0
f)	**C–H···F**	M06-2X/6-31G**	-2.3	-1.3	3.8	-2.0	-2.8
		M06-2X-D3/6-31G**	-3.9	-1.3	3.8	-2.0	-4.4

Table S4. A Comparison of the Total Interaction Energies (in kcal/mol) between the Catalyst (via its fragments **A** or **B**) and the Substrate in the TSs Calculated using the Respective Model Systems at M06-2X and M06-2X-D3 Levels of Theory (**M3**)[a] and the PIEDA Methods (**M2**). The BSSE corrected values are given in parenthesis

type of interaction (χ_{i-q})	no. of contacts (N_{i-q})	total interaction energy (M3)		total interaction energy (PIEDA) (M2)	
		M06-2X	M06-2X-D3	M06-2X	M06-2X-D3
TS-I-S					
C–H···O	2	-2.6 (-1.4)	-2.6 (-1.4)	-2.8	-4.0
lp(O)···π	1	-4.7 (-2.9)	-4.9 (-3.0)	-5.1	-7.9
C–H··· π	2	-3.2 (-2.2)	-3.8 (-2.6)	-3.4	-8.6
Total:		-10.5 (-6.5)	-11.3 (-7.0)	-11.3	-20.5
TS-I-R					
lp(O)···π	1	-4.7 (-2.9)	-4.9 (-3.0)	-5.1	-7.9
C–H··· π	2	-3.2 (-2.2)	-3.8 (-2.6)	-3.4	-8.6
Total:		-7.9 (-5.1)	-8.7 (-5.6)	-8.5	-16.5

TS-IIa-R					
C–H⋯O	1	-1.3 (-0.7)	-1.3 (-0.7)	-1.4	-2.0
lp(O)⋯π	1	-4.7 (-2.9)	-4.9 (-3.0)	-5.1	-7.9
C–H⋯ π	2	-3.2 (-2.2)	-3.8 (-2.6)	-3.4	-8.6
C–H⋯F	6	-13.8 (-3.6)	-13.8 (-4.2)	-13.8	-23.4
C–F⋯O	5	-5.2 (-0.7)	-5.7 (-1.2)	-5.2	-10.7
Total:		-28.2 (-10.1)	-29.5 (-11.7)	-28.9	-52.6
TS-IIa-S					
C–H⋯O	1	-1.3 (-0.7)	-1.3 (-0.7)	-1.4	-2.0
lp(O)⋯π	2	-9.4 (-5.8)	-9.8 (-6.0)	-10.2	-15.8
C–H⋯ π	1	-1.6 (-1.1)	-1.9 (-1.3)	-1.7	-4.3
C–H⋯F	4	-9.2 (-2.4)	-9.2 (-2.8)	-9.2	-15.6
C–F⋯O	4	-4.1 (-0.5)	-4.5 (-0.9)	-4.1	-8.5
Total:		-25.6 (-10.5)	-26.7 (-11.7)	-26.6	-46.2
TS-IIb-R					
C–H⋯O	1	-1.3 (-0.7)	-1.3 (-0.7)	-1.4	-2.0
C–H⋯ π	6	-9.6 (-6.6)	-11.4 (-7.8)	-10.2	-25.8
Total:		-10.9 (-7.3)	-12.7 (-8.5)	-11.6	-27.8
TS-IIb-S					
lp(O)⋯π	3	-14.1 (-8.7)	-14.7 (-9.0)	-15.3	-23.7
C–H⋯ π	3	-4.8 (-3.3)	-5.7 (-3.9)	-5.1	-12.9
Total:		-18.9 (-12.0)	-20.4 (-12.9)	-20.4	-36.6
TS-IIIa-S					
O–H⋯ π	1	-4.2 (-3.3)	-4.3 (-3.4)	-4.5	-7.1
lp(O)⋯π	1	-4.7 (-2.9)	-4.9 (-3.0)	-5.1	-7.9
C–H⋯ π	3	-4.8 (-3.3)	-5.7 (-3.9)	-5.1	-12.9
Total:		-13.7 (-9.5)	-14.9 (-10.3)	-14.7	-27.9
TS-IIIb-R					
O–H⋯ π	1	-4.2 (-3.3)	-4.3 (-3.4)	-4.5	-7.1
lp(O)⋯π	1	-4.7 (-2.9)	-4.9 (-3.0)	-5.1	-7.9
C–H⋯ π	3	-4.8 (-3.3)	-5.7 (-3.9)	-5.1	-12.9
Total:		-13.7 (-9.5)	-14.9 (-10.3)	-14.7	-279

[a] Basis set used is 6-31G**, the interaction energies in the respective model binary systems, bound primarily by one type of NCI (i, j, k, …), computed using the supermolecular approach (Figure S3) are summed up using $N_i\chi_i + N_j\chi_j + \ldots + N_q\chi_q$ where χ_{i-q} are individual interactions of each type and N_{i-q} is the number interactions of a given type.

6. Probing the Potential Origin of High Charge Transfer and Exchange Energies Noticed in Reaction IIb

In the case of reaction **IIb**, a notably higher charge transfer and exchange energies between 3,3'-substituents of the catalyst and the substrate are identified. It is important to note that due to the convergence issues encountered during the calculation of the energies of the fragment pairs (as shown in the partition scheme in Scheme 1), the initial guess for the density matrix

of the fragments are chosen using the hybrid orbital projection and the RHF for each dimer, prior the DFT runs the TSs of reaction **IIb**. This approach is therefore different from the default method, where the initial guess density matrix of the fragment pair is taken as the sum of converged densities/orbitals of the monomers.

This might be the cause of high charge transfer and repulsive energies noted in reaction **IIb**, whilst the total interaction energies remain reasonable. These *intramolecular* energies, as evaluated through our FMO protocol, is compared with the corresponding values obtained using an alternative approach that uses a partition scheme to transform the problem to an *intermolecular* interaction energy, wherein the same method of constructing the guess orbitals for the dimers as in the intramolecular case was used. In the latter method, interaction energies between fragments with hydrogen capping (wherein the C–C bond between the 3,3'-substituents and the backbone of the catalyst is capped with a H atom) are estimated using a supermolecular approach (Figure S4).[5,6,7]

(5) Wheeler, S. E.; Houk, K. N. Substituent Effects in the Benzene Dimer Are Due to Direct Interactions of the Substituents with the Unsubstituted Benzene. *J. Am. Chem. Soc.* **2008**, *130*, 10854–10855.

(6) Wheeler, S. E.; Bloom, J. W. G. Toward a More Complete Understanding of Noncovalent Interactions Involving Aromatic Rings. *J. Phys. Chem. A* **2014**, *118*, 6133–6147.

(7) Wheeler, S. E. Understanding Substituent Effects in Noncovalent Interactions Involving Aromatic Rings. *Acc. Chem. Res.* **2013**, *46*, 1029–1038.
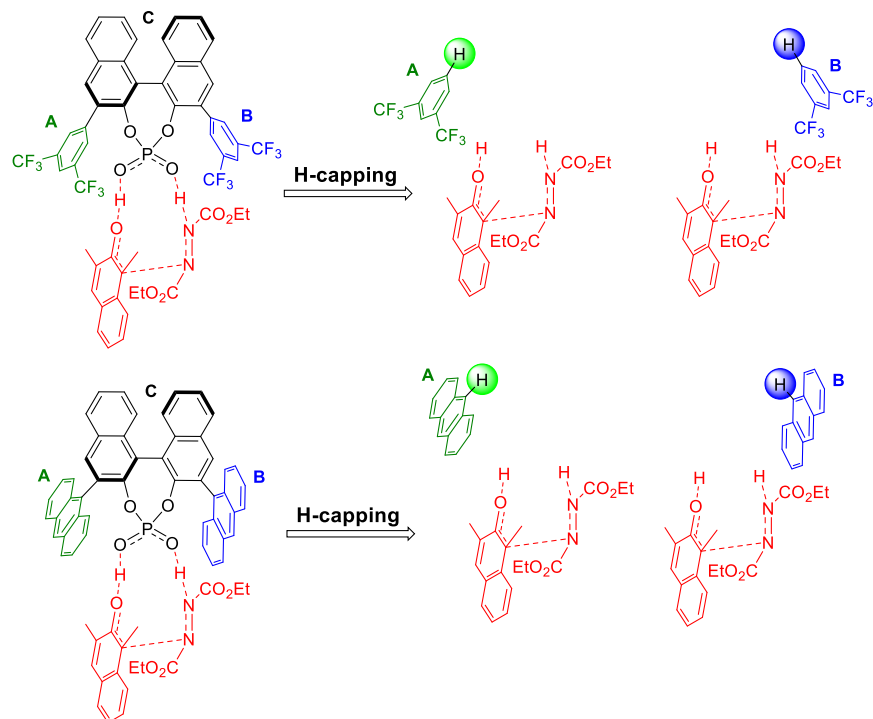
Figure S4. Illustration of how the H-capped fragments are generated in the case of reactions **IIa** and **IIb**
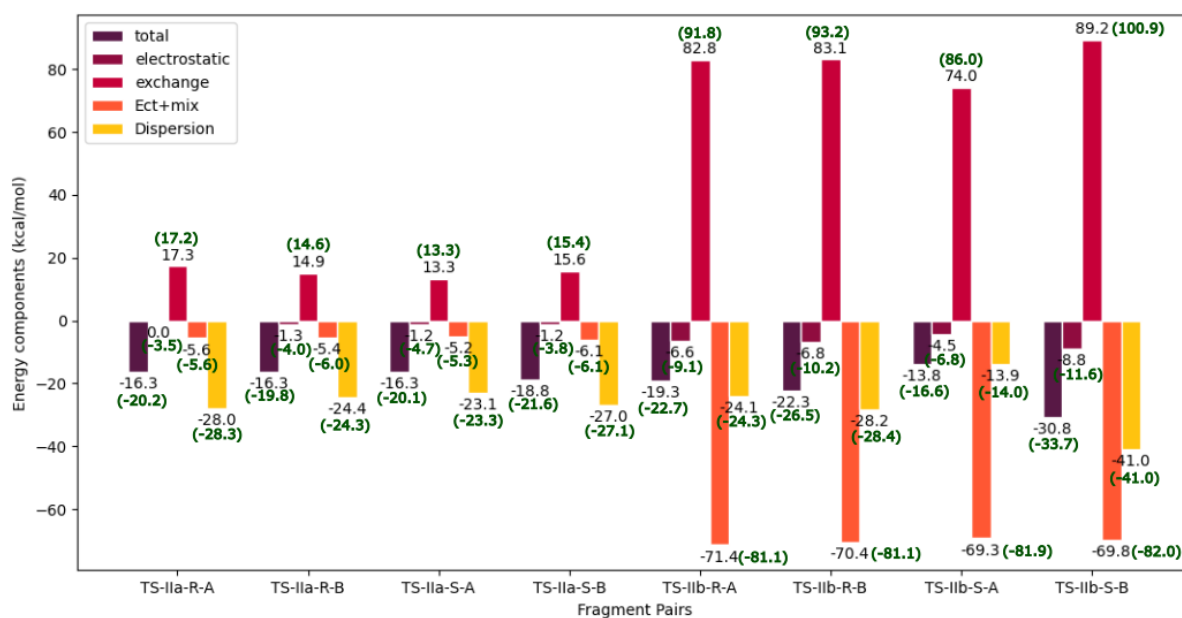
Figure S5. Comparison of various components of the total interaction energies as obtained using PIEDA and H-capping (shown in parentheses) methods in the case of reactions **IIa** and

IIb.

It is evident from Figure S5 that the magnitude of the total interaction energies obtained using the H-capping method is generally higher by about 4 kcal/mol. Among the constituents, the dispersion energies given by the FMO as well as the H-capping methods in both reaction **IIa** and **IIb** are nearly the same, so are the charge transfer and repulsive exchange energies in the case of reaction **IIa**. This indicates that replacing the CPA backbone with a hydrogen atom does not significantly impact the dispersion energies in both the reactions, and on the charge transfer and exchange energies estimates for reaction **IIa**, where the substituent is relatively electron deficient. The major difference between the FMO and H-capping methods is noted in the electrostatic energies, where the H-capped method generally yields a higher value (more negative). This prediction can be reconciled as the electron density on both fragments will be altered upon replacing the anionic CPA backbone by a capping hydrogen atom for evaluating the 'intermolecular' interactions between the 3,3'-substituents of CPA and the substrate. With the anthryl fragment, the exchange and charge transfer energies calculated using H-capping display significant difference with that calculated using FMO. The repulsive interactions are expected to increase with an electron rich substituent such as an anthryl group, as opposed to when the 3,3' positions are occupied by $3,5-(CF_3)_2-C_6H_3$ group.

In order to examine whether the initial guess density matrix of the fragment pairs is the cause of such high energies, two binary super systems; DEAD···anthracene as well as DEAD···pyrene, were optimized at the M06-2X/6-31G** level of theory. The FMO2 calculations were performed on these systems by using the default initial guess densities. The data given in Table S5 reveals that the charge transfer and repulsive exchange energies in these intermolecular binary aggregates are more reasonable. However, these are still on the higher side than the corresponding energetic terms noted in the case of reaction **IIa**. Further,

to make sure that the charge transfer energies are not an artifact of the functional, the long range corrected CAM-B3LYP along with the D3 corrections is employed.[8,9] The charge transfer and repulsive energies are found to be consistent between the CAM-B3LYP-D3 and the other functionals.

It is therefore clear that the initial guess of the density matrix for the dimer fragments is important. Once the solution to each fragment is achieved, the fragment pair densities are not self-consistently optimized in the FMO formalism. In spite of the overestimation of charge transfer and exchange energies due to the deficiency in the guess densities, our inference that the charge transfer makes a higher contribution to the interaction energy between DEAD and anthracene holds good. This could be verified by comparing the corresponding values as noted for the independent computations on optimized model binary complexes between DEAD and anthracene. A similar trend was also found in the case of pyrene and DEAD.

(8) Yanai, T.; Tew, D.; Handy, N. A new hybrid exchange-correlation functional using the Coulomb-attenuating method (CAM-B3LYP). *Chem. Phys. Lett.* **2004**, *393*, 51-57.

(9) Grimme, S.; Antony, J.; Ehrlich, S.; Krieg, H. A consistent and accurate ab initio parametrization of density functional dispersion correction (DFT-D) for the 94 elements H-Pu. *J. Chem. Phys.* **2010**, *132*, 154104 .

Table S5. The PIEDA Interaction Energies and Constituent Decomposed Energy Terms Calculated for a) Anthracene and b) Pyrene with DEAD Fragment at the M06-2X/6-31G**, M06-2X-D3/6-31G**, CAM-B3LYP/6-31G** and CAM-B3LYP-D3/6-31G** Level of Theories

a)					b)			
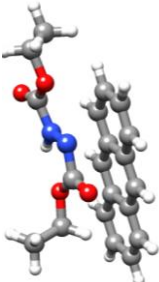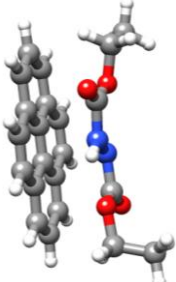
	Level of theory	Total	Elst.	Exch.	Ect+mix	Disp.
a	M06-2X/6-31G**	-45.6	-34.5	49.7	-25.8	-35.0
	M06-2X-D3/6-31G**	-64.9	-34.5	49.7	-25.8	-54.3
	CAM-B3LYP/6-31G**	-34.9	-33.3	41.4	-29.3	-13.7
	CAM-B3LYP-D3/6-31G**	-54.2	-33.3	41.4	-29.3	-33.0
b	M06-2X/6-31G**	-41.9	-31.0	46.7	-18.8	-38.7
	M06-2X-D3/6-31G**	-64.3	-31.0	46.7	-18.8	-61.2
	CAM-B3LYP/6-31G**	-28.7	-29.9	37.8	-22.1	-14.5
	CAM-B3LYP-D3/6-31G**	-51.1	-29.9	37.8	-22.1	-36.9

7. Interaction Energies in Reaction IIa Involving CPA Backbone Fragment
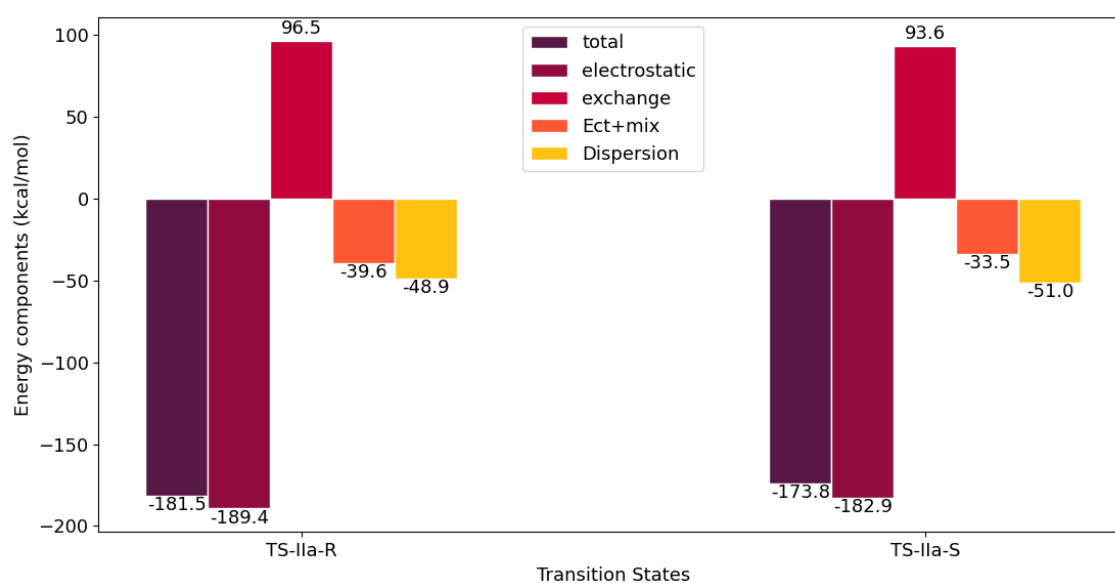
Figure S6. The PIEDA interaction energies and its components between the TS reactant fragment and CPA backbone in reaction **IIa**.

8. Topological Maps using Atoms In Molecules Approach
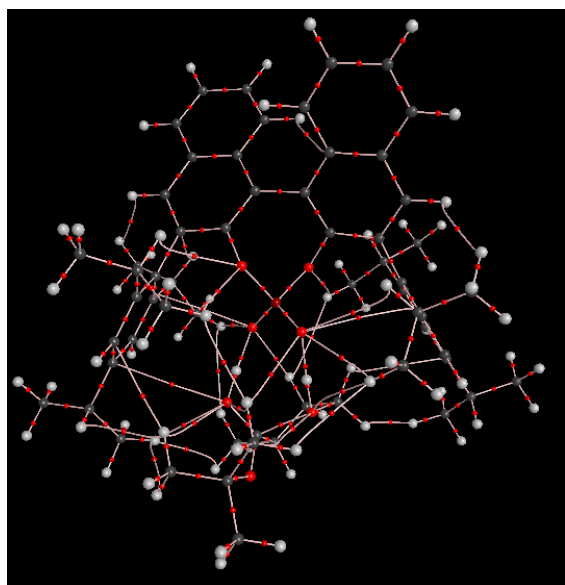
TS-I-S
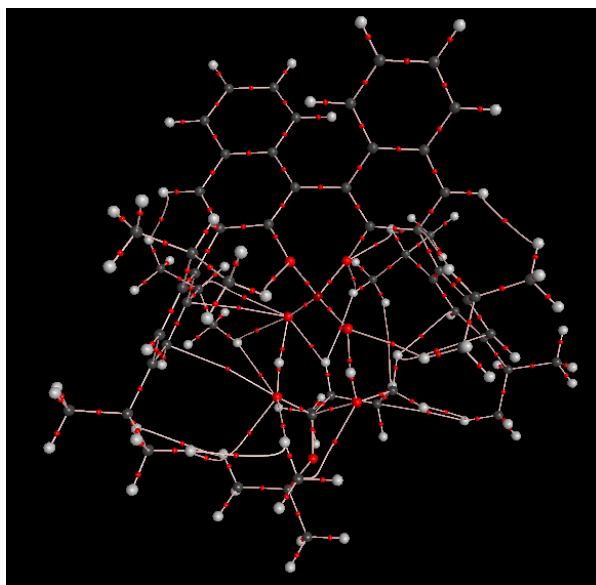
TS-I-R
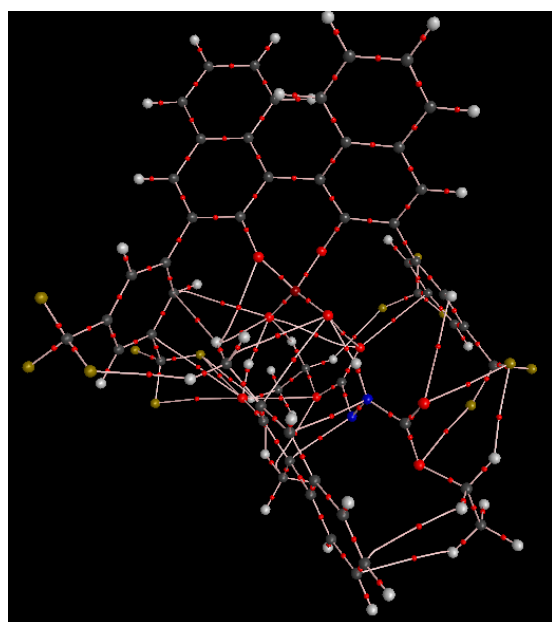
TS-IIa-S
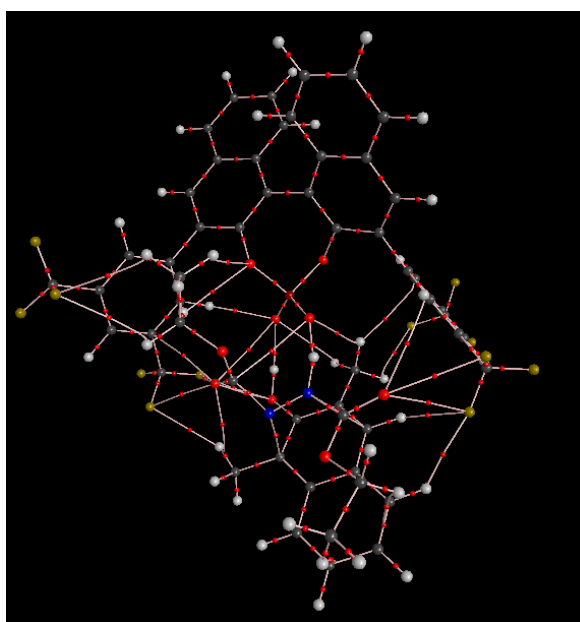
TS-IIa-R

Figure S7 continued…
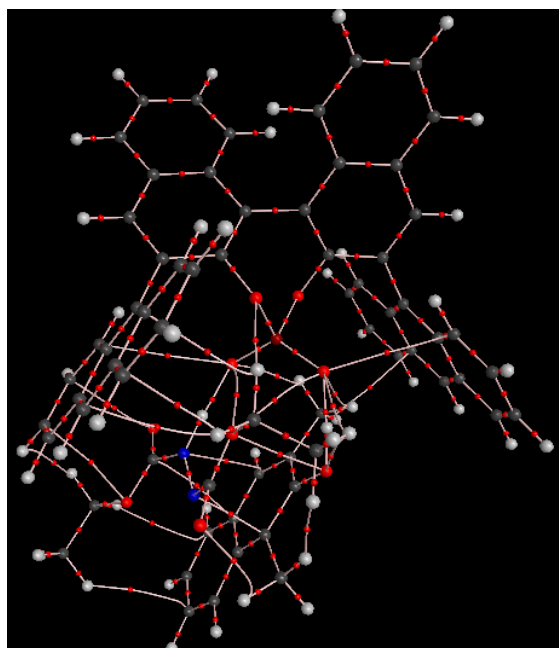
TS-IIb-S
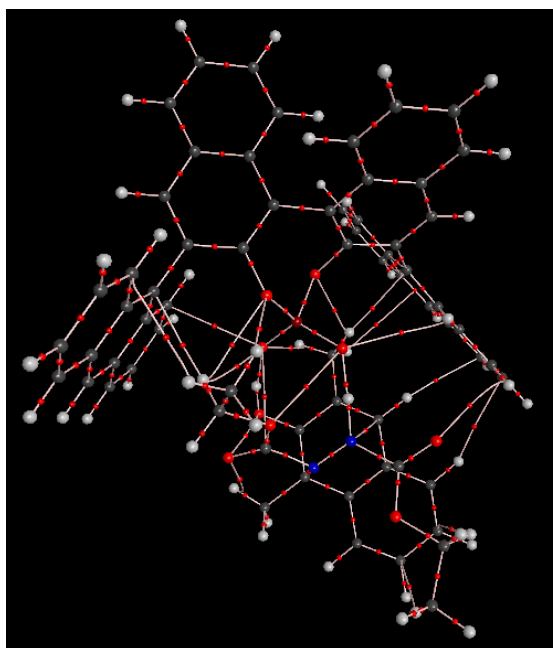
TS-IIb-R
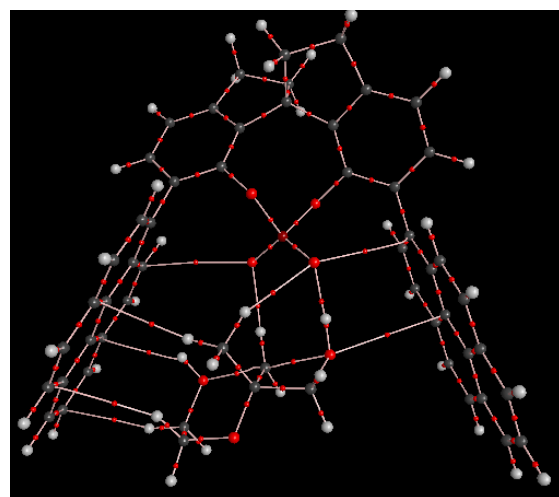
TS-IIIa-S
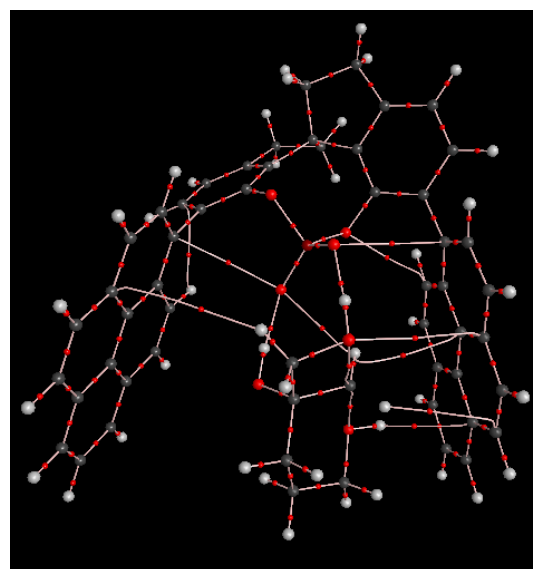
TS-IIIb-R

Figure S7. The topological map of the TSs as per the AIM formalism. The red dots represent the (3,-1) bond critical points (bcps).